Giant Spin-Driven Ferroelectric Polarization in BiFeO$_3$ at Room Temperature

Jun Hee Lee[*] and Randy S. Fishman

Materials Science and Technology Division, Oak Ridge National Laboratory, Oak Ridge, Tennessee 37831, USA
(Received 24 April 2015; published 11 November 2015)

The spin-driven polarizations of type-I multiferroics are veiled by the preexisting ferroelectric (FE) polarization. Using first-principles calculations combined with a spin model, we uncover two hidden but huge spin-driven polarizations in the room-temperature multiferroic BiFeO$_3$. One is associated with the global inversion symmetry broken by a FE distortion, and the other is associated with the local inversion symmetry broken by an antiferrodistortive octahedral rotation. Comparison with recent neutron scatterings reveals tha first polarization reaches ~ 3.0 μC/cm^2, which is larger than in any other multiferroic material. Our exhaustive study paves a way to uncover the various magnetoelectric couplings that generate hidden spin-driven polarizations in other type-I multiferroics.

Although BiFeO$_3$ is endowed with high ferroelectric (FE) and antiferromagnetic (AFM) transition temperatures, $T_c \approx$ 1100 K [1] and $T_N \approx 640$ K [2], the disparity between T_c and $T_N \ll T_c$ in this type-I multiferroic suggests that the magnetoelectric (ME) couplings may be quite weak. Despite enormous effort [2–6], a microscopic picture embracing all the ME coupling mechanisms in bulk BiFeO$_3$ is still missing. By contrast with type-II multiferroics, where $T_N = T_c$ and the ME polarizations have been well characterized [7], the large FE polarization, high Néel temperature, and long 62 nm period of BiFeO$_3$ have hindered measurement of its spin-driven ME polarization. Based on elastic [6,8] and inelastic neutron-scattering [9], Raman-scattering [10], and terahertz spectroscopy [11] measurements of recently available single crystals, it is now possible to provide detailed information about the intrinsic ME couplings in bulk BiFeO$_3$. These results are crucial to control the electrical properties of BiFeO$_3$ with a magnetic field and vice versa.

Combining a first-principles approach with a spin-cycloidal model, we explain the origin of all possible ME couplings and spin-driven (SD) polarizations produced by exchange-striction (ES), spin-current (SC), and single-ion anisotropy (SIA). All polarizations are fostered by broken inversion symmetries with two types of lattice distortions in $R3c$ bulk BiFeO$_3$: FE and antiferrodistortive (AFD). By comparing our results for the spin-driven atomic displacements with elastic neutron-scattering measurements [6,8,12], we demonstrate that the ES polarization (ESP) ~ 3 μC/cm^2 dominates over other sources of polarization in the spin cycloid and is larger than any previously reported SD polarization.

In type-I multiferroics, the absence of an inversion center due to the preexisting FE polarization fosters the SD polarizations. Specifically, the change of the scalar product $\mathbf{S}_i \cdot \mathbf{S}_j$ at the magnetic transition modulates the degree of broken-inversion symmetry and produces the corresponding ESPs [13]. While the FE distortion eliminates a

global-inversion center, the AFD distortion eliminates a local-inversion center. Therefore, FE and AFM distortions each generate their own ESP.

All possible polarizations are obtained by differentiating the Hamiltonian with respect to an electric field. For symmetric exchange couplings, ES is dominated by the response of the nearest-neighbor interaction J_1 from the original Hamiltonian:

$$\mathcal{H}^{\mathrm{EX}} = -\sum_{\langle i,j \rangle} J_1 \mathbf{S}_i \cdot \mathbf{S}_j = -\sum_{\mathbf{R}_i, \mathbf{R}_j = \mathbf{R}_i + \mathbf{e}_k} J_1^k \mathbf{S}_i \cdot \mathbf{S}_j, \quad (1)$$

where $k = x$, y, or z. Taking the FE polarization along $\mathbf{z}' = [111]$, the ESPs are then obtained from $\boldsymbol{P}^{\mathrm{ES}} = -\vec{\nabla}_{\vec{E}} \mathcal{H}^{\mathrm{EX}}/N$ with

$$\boldsymbol{P}^{\mathrm{ES}}_{\mathrm{FE}} = \mathbf{z}'(\mathbf{z}' \cdot \boldsymbol{P}^{\mathrm{ES}})$$
$$= \mathbf{z}'(2C_\perp + C_\parallel)\mathbf{z}' \cdot \mathbf{W}_1 = \mathbf{z}'\sqrt{3}C_{\mathrm{FE}}\mathbf{z}' \cdot \mathbf{W}_1, \quad (2)$$
$$\boldsymbol{P}^{\mathrm{ES}}_{\mathrm{AFD}} = \mathbf{z}' \times \boldsymbol{P}^{\mathrm{ES}}$$
$$= (C_\parallel - C_\perp)\mathbf{z}' \times \mathbf{W}_2 = C_{\mathrm{AFD}}\mathbf{z}' \times \mathbf{W}_2, \quad (3)$$
$$W_{1k} = \frac{1}{N}\sum_{\mathbf{R}_i, \mathbf{R}_j = \mathbf{R}_i + \mathbf{e}_k} \mathbf{S}_i \cdot \mathbf{S}_j, \quad (4)$$
$$W_{2k} = \frac{1}{N}\sum_{\mathbf{R}_i, \mathbf{R}_j = \mathbf{R}_i + \mathbf{e}_k} (-1)^{n_i}\mathbf{S}_i \cdot \mathbf{S}_j, \quad (5)$$

where $C_\perp = \partial J_1^\beta/\partial E_\alpha$ ($\beta \neq \alpha$) and $C_\parallel = \partial J_1^\alpha/\partial E_\alpha$ for spin bonds perpendicular and parallel to the electric field, respectively.

Unlike W_{1k}, W_{2k} alternates in sign due to opposing AFD rotations on adjacent hexagonal layers labeled by n_i. The ESP parallel to $\mathbf{z}'$ with coefficient $C_{\mathrm{FE}} = (2C_\perp + C_\parallel)/\sqrt{3}$ modulates the FE polarization that already breaks inversion symmetry above T_N; the ESP perpendicular to $\mathbf{z}'$ has coefficient $C_{\mathrm{AFD}} = C_\perp - C_\parallel$. The AFD breaks the local

inversion between nearest-neighbor spins perpendicular to $\mathbf{z}'$ because each oxygen moves along $[0,\bar{1},1]$, $[1,0,\bar{1}]$, and $[\bar{1},1,0]$, perpendicular to $\mathbf{z}'$.

By ignoring the cycloidal harmonics but including the tilt [14] τ produced by $\boldsymbol{D}_{\mathrm{AFD},k}$, the spin state propagating along one of the three hexagonal orientations $\mathbf{x}'$ can be approximated [15] as

$$S_{x'}(\mathbf{R}_i) = S(-1)^{n_i+1}\cos\tau \sin[2\sqrt{2}\pi\delta\mathbf{x}'\cdot\mathbf{R}_i/a], \quad (6)$$

$$S_{y'}(\mathbf{R}_i) = S\sin\tau \sin[2\sqrt{2}\pi\delta\mathbf{x}'\cdot\mathbf{R}_i/a], \quad (7)$$

$$S_{z'}(\mathbf{R}_i) = S(-1)^{n_i+1}\cos[2\sqrt{2}\pi\delta\mathbf{x}'\cdot\mathbf{R}_i/a], \quad (8)$$

where $a = 3.96$ Å is the pseudocubic lattice constant and $\delta/(\sqrt{2}a) = 62$ nm is the period of the cycloid so that $\delta \approx 0.0045$. Recall that [16] $\sin\tau = S_0/S$, where $M_0 = 2\mu_B S_0$ is the weak FM moment of the AFM phase along $\mathbf{y}'$ above H_c. For a moment [3] $M_0 = 0.03\mu_B$, $\tau = 0.006$ or $0.34°$. Because higher harmonics $C_{2n+1>1}$are neglected, averages taken with the tilted cycloid introduce a very small error of order $C_3^2 \approx 2.5\times10^{-5}$.

To calculate the electric-field-induced lattice distortion and the associated change in J_1, we employ a method [17] that was successfully applied to other multiferroic oxides. The resulting ESP coefficients are given in Table I. Using the result $C_{\mathrm{FE}} = 215$ nC/cm^2 and Eq. (2) for $\mathbf{P}_{\mathrm{FE}}^{\mathrm{ES}}$, we find that the ESP for the simple twisted cycloid in Eqs. (6)–(8) is

$$\langle\mathbf{P}_{\mathrm{FE}}^{\mathrm{ES}}\rangle = -C_{\mathrm{FE}}S^2\mathbf{z}'\cos^2\tau = -1.3\ \mu\mathrm{C/cm}^2\mathbf{z}'. \quad (9)$$

Because a harmonic approximation [17] was used to generate the possible polar distortions induced by the electric field, this ESP was evaluated only to quadratic order in the lattice distortions driven by the spin ordering.

However, the ESP may be large enough to induce atomic displacements and lattice distortions beyond the harmonic limit. As shown in Fig. 1, one can calculate the ESP more accurately including anharmonic effects and spin-lattice couplings by fully relaxing the atoms and the lattice for different magnetic orderings (G-AFM and FM) with

$$\Delta P_{\mathrm{FE}}^{\mathrm{ES}} = P_{\mathrm{FM}} - P_{\mathrm{AFM}} = 2C_{\mathrm{FE}}S^2$$
$$= \frac{1}{V}\sum_{i=\mathrm{Fe,Bi}}\{Z_{i,\mathrm{FM}}^* u_{i,\mathrm{FM}} - Z_{i,\mathrm{AFM}}^* u_{i,\mathrm{AFM}}\}$$
$$= 6.0\ \mu\mathrm{C/cm}^2, \quad (10)$$

TABLE I. Calculated (LSDA + U) ESP components perpendicular $C_\perp$ or parallel $C_\parallel$ to the electric field and associated FE (C_{FE}) and AFD (C_{AFD}) SD polarization. Values in the parentheses are directly obtained from the polarization difference of the relaxed structures with G-AFM or FM ordering as shown in Eqs. (10) and (12) and Fig. 1.

nC/cm^2	$C_\perp$	$C_\parallel$	C_{FE}	C_{AFD}
LSDA + U	186	0.769	215 (480)	−185 (−108)

so that $C_{\mathrm{FE}} = 480$ nC/cm^2 and

$$\langle\mathbf{P}_{\mathrm{FE}}^{\mathrm{ES}}\rangle = -C_{\mathrm{FE}}S^2\mathbf{z}'\cos^2\tau = -3.0\ \mu\mathrm{C/cm}^2\mathbf{z}', \quad (11)$$

where Z_i^*, u_i, and V represent the Born effective charge, atomic position, and volume, respectively. The change of spin ordering from G-AFM to FM shifts the Fe and Bi atoms by 0.020 and 0.019 Å, respectively, as shown in Fig. 1. While the Bi effective charge hardly changes ($Z_{\mathrm{AFM}}^* = 4.82e$, $Z_{\mathrm{FM}}^* = 4.83e$), the Fe effective charge changes significantly ($Z_{\mathrm{AFM}}^* = 3.91e$, $Z_{\mathrm{FM}}^* = 4.11e$) due to the SD hybridization between Fe and oxygen. Consequently, $C_{\mathrm{FE}} = 480$ nC/cm^2 is a factor of 2 larger than the harmonic value in Table I. This result will later be compared with neutron-scattering measurements.

Supplemental Material [18] shows that Eq. (3) describes the ESP perpendicular to the FE-polarization direction $\mathbf{z}'$ due to the inversion-symmetry breaking from AFD rotations. Hence, the second ESP reflects the change of AFD distortions and the associated local polarization driven by spins perpendicular to $\mathbf{z}'$. For a simple tilted cycloid, $\langle W_{2k}\rangle = \langle P_{\mathrm{AFD}}^{\mathrm{ES}}\rangle = 0$, because the AFD distortions do not globally break inversion symmetry.

As shown in Fig. 1, first-principles calculations can capture $P_{\mathrm{AFD}}^{\mathrm{ES}}$ by evaluating the AFD-induced oxygen displacements perpendicular to $\mathbf{z}'$ with the change of spin ordering. The increase of the AFD rotation ($\Delta\theta = 0.54°$) from G-AFM ($\theta = 13.08°$) to FM ($\theta = 13.62°$) corresponds to an increase of the oxygen displacement (0.015 Å) along $[0,-1,1]$, $[1,0,-1]$, and $[-1,1,0]$ perpendicular to $\mathbf{z}'$. Therefore,

$$\Delta P_{\mathrm{AFD}}^{\mathrm{ES}} = P_{\mathrm{FM}} - P_{\mathrm{AFM}} = 2C_{\mathrm{AFD}}S^2$$
$$= \frac{-3.30e}{V}0.015\ \text{Å} = -1340\ \mathrm{nC/cm}^2, \quad (12)$$
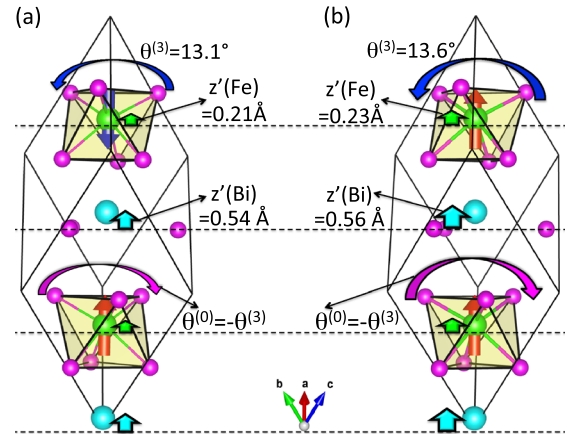
FIG. 1 (color online). First-principles relaxation results for magnetic orderings (a) G-AFM → $P = 93\ \mu\mathrm{C/cm}^2$ and (b) FM → $P = 99\ \mu\mathrm{C/cm}^2$ to calculate ESPs from FE distortion of Fe [$\mathbf{z}'$(Fe)] and of Bi [$\mathbf{z}'$(Bi)] along [111] and AFD R_4^+ rotations (θ) perpendicular to [111]. (0) and (3) are indices of hexagonal layers ($x + y + z = n$).

so that $C_{\mathrm{AFD}} = -108$ nC/cm^2.

Interestingly, the two ESPs C_{FE} and C_{AFD} are coupled. While the ESP components $C_\perp$ and $C_\parallel$ cooperatively increase ESP along $\mathbf{z}'$ under the inversion symmetry broken by FE, they produce opposite contributions to the AFD-induced ESP perpendicular to $\mathbf{z}'$. $C_\perp$ is largely positive due to the reduction of the Fe-O-Fe bond angle driven by the FE distortion, which favors FM from the Goodenough-Kanamori (GK) rules [24]; $C_\parallel$ is almost zero because the bond contraction between Fe-O-Fe does not significantly alter the spin-density environment around the d^5 electrons of Fe. The large difference between $C_\perp$ and $C_\parallel$ induces the large ESP induced by AFD rotations.

The global- and local-inversion-symmetry breaking by FE and AFD distortions produce the DM interactions $\boldsymbol{D}_{\mathrm{FE},k}$ and $\boldsymbol{D}_{\mathrm{AFD},k}$. Because of their distinct translational characters, they can be separated using the procedure sketched in Fig. 2. Since the FE distortion is globally uniform, its associated $\boldsymbol{D}_{\mathrm{AFD},k}$ is uniform, too. Because the AFD rotation alternates between hexagonal layers, the associated DM vector $\boldsymbol{D}_{\mathrm{AFD},k}$ also alternates, as shown by the blue arrows in Fig. 2. As shown in Figs. 2(a) and 2(b), show that a cycloid consisting of four spins along $\mathbf{e}_k$ generates a translation-invariant spin current $\mathbf{S}_i \times \mathbf{S}_j$. The uniform component $\boldsymbol{D}_{\mathrm{FE},k}$ is extracted from

$$E_{\mathrm{FE},k}^{\pm,\gamma} = E_0 \pm 4D_{\mathrm{FE},k}^\gamma S^2 - \frac{4}{3}KS^2, \qquad (13)$$

$$D_{\mathrm{FE},k}^\gamma = \frac{1}{8S^2}(E_{\mathrm{FE},k}^{+,\gamma} - E_{\mathrm{FE},k}^{-,\gamma}), \qquad (14)$$

where $\pm$ refer to counterclockwise ($+$) and clockwise ($-$) rotations, respectively. The translation-odd $\boldsymbol{D}_{\mathrm{AFD},k}$ does not appear in this expression.

By using a zigzag-type spin arrangement that generates a spin current $\mathbf{S}_i \times \mathbf{S}_j$ with alternating sign, the translation-odd $\boldsymbol{D}_{\mathrm{AFD},k}$ is extracted from

$$E_{\mathrm{AFD},k}^{\pm,\gamma} = E_0 \pm 4D_{\mathrm{AFD},k}^\gamma S^2 - \frac{4}{3}KS^2, \qquad (15)$$

$$D_{\mathrm{AFD},k}^\gamma = \frac{1}{8S^2}(E_{\mathrm{AFD},k}^{+,\gamma} - E_{\mathrm{AFD},k}^{-,\gamma}), \qquad (16)$$

which does not contain the translation-even $\boldsymbol{D}_{\mathrm{FE},k}$.

As for the ESP, the SC polarization (SCP) $\mathbf{P}^{\mathrm{SC}} = \mathbf{P}^{\mathrm{SC}}_{\mathrm{FE}} + \mathbf{P}^{\mathrm{SC}}_{\mathrm{AFD}}$ splits into terms produced by the inversion-symmetry breaking of FE and AFD distortions, respectively. The first SCP is caused by the response of the FE distortion to an electric field:

$$
\begin{aligned}
P^{\mathrm{SC}}_{\mathrm{FE},\gamma} &= -\frac{\partial \mathcal{H}^{\mathrm{SC}}_{\mathrm{FE}}}{\partial E_\gamma} \\
&= -\frac{1}{N}\sum_{\mathbf{e}_k} \frac{\partial \boldsymbol{D}_{\mathrm{FE},k}}{\partial E_\gamma} \cdot (\mathbf{S}_i \times \mathbf{S}_{i+\mathbf{e}_k}).
\end{aligned}
\qquad (17)
$$

The E-field derivatives of the DM, $\mathbf{f}^{k\beta} = \partial \boldsymbol{D}_{\mathrm{FE},k}/\partial E_\beta$, are presented in Table II and Supplemental Material [18].

The second SCP arises from the AFD rotation. Its sign alternates due to the alternating AFD rotation direction alongis extracted from [111]:

$$
\begin{aligned}
P^{\mathrm{SC}}_{\mathrm{AFD},\gamma} &= -\frac{\partial \mathcal{H}^{\mathrm{SC}}_{\mathrm{AFD}}}{\partial E_\gamma} \\
&= -\frac{1}{N}\sum_{\mathbf{e}_k} (-1)^{n_i} \frac{\partial \boldsymbol{D}_{\mathrm{AFD},k}}{\partial E_\gamma} \cdot (\mathbf{S}_i \times \mathbf{S}_{i+\mathbf{e}_k}).
\end{aligned}
\qquad (18)
$$

The SCP components $\mathbf{a}^{k\beta} = \partial \boldsymbol{D}_{\mathrm{AFD},k}/\partial E_\beta$ are evaluated in Supplemental Material [18] and presented in Table II.

SIA is the last possible source for the ME polarization. Starting with the SIA energy $\mathcal{H}^{\mathrm{SIA}} = -K\sum_i(\mathbf{S}_i \cdot \mathbf{z}')^2$, the SD polarization has the $\mathbf{z}'$ component

$$\mathbf{z}' \cdot \mathbf{P}^{\mathrm{SIA}} = \frac{\sqrt{3}\xi}{N}\sum_i(\mathbf{S}_i \cdot \mathbf{z}')^2, \qquad \xi = \frac{\partial K}{\partial E_\alpha}. \qquad (19)$$

The elongation ξ of K is given in Table II.

For the simple tilted cycloid of Eqs. (6)–(8),

$$\langle \mathbf{P}^{\mathrm{SIA}} \rangle = \frac{\sqrt{3}}{2N}\xi S^2 \mathbf{z}', \qquad (20)$$

$$
\begin{aligned}
\langle \mathbf{P}^{\mathrm{SC}}_{\mathrm{FE}} \rangle = &-2\pi\sqrt{6}S^2\delta\cos\tau \\
&\times \{(f_y^{xx} - f_y^{xy})\mathbf{y}' + \sqrt{2}(f_z^{xy} - f_y^{xy} - f_y^{xx})\mathbf{z}'\},
\end{aligned}
\qquad (21)
$$

FIG. 2 (color online). Separation of FE ($\boldsymbol{D}_{\mathrm{FE},k}$) and AFD ($\boldsymbol{D}_{\mathrm{AFD},k}$) DM interactions in BiFeO$_3$. Spin directions (red arrows) and DM vectors (blue arrows) are indicated. (a) and (b) have clockwise and counterclockwise rotation, respectively, of spins and use an 80 atom unit cell (four spins in the unit cell along each direction). (c) and (d) have zigzag-type spin ordering. $\pm$ above red arrows denote signs of DM interaction and of spin current between two nearest-neighbor spins.

TABLE II. Calculated (LSDA + U) SCPs and SIA polarization (SIAP) derived from DM and K interactions. Subscripts denote whether the spin-bond direction is parallel or perpendicular to the electric field. f_z^{xy} and f_y^{xy} are not shown due to low convergence.

nC/cm²	SCP from D						SIAP
	a_x^{xx}	a_y^{xx}	a_y^{xy}	a_x^{xy}	a_z^{xy}	f_y^{xy}	ξ
LSDA + U	6.6	−21	16	1.2	−13	−4.9	16

$$\langle \mathbf{P}_{AFD}^{SC} \rangle = -S^2 \sin 2\tau \left\{ \frac{a_x^{xx}}{2} + a_y^{xx} + a_x^{xy} + a_y^{xy} + a_z^{xy} \right\} \mathbf{z}'.$$

(22)

Symmetry relations for $f_\gamma^{\alpha\beta}$ and $a_\gamma^{\alpha\beta}$ are given in Supplemental Material [18]. Because $\delta, \tau \ll 1$, the projected polarization along $\mathbf{z}'$ is $\mathbf{z}' \cdot \langle \mathbf{P}^{SC} + \mathbf{P}^{SIA} \rangle \approx \mathbf{z}' \cdot \langle \mathbf{P}^{SIA} \rangle \approx 87$ nC/cm², which is larger than the experimental value 40 nC/cm² [3,4] obtained from the jump in polarization below the critical field $H_c \approx 20$ T. Intriguingly, $\mathbf{D}_{FE,k}$ produces an additional SCP along $\mathbf{y}'$, which may explain why the SC also generates a polarization perpendicular to $\mathbf{z}'$ [4]. Since the SCP and SIAP are still much smaller than the ESP, the dominant polarization at the magnetic transition is driven by ES.

Figure 3 shows all the ME polarizations driven by the AFM spin ordering around T_N and compares those results to elastic neutron-scattering measurements [6,8,12]. Although the neutron-scattering data are rather spread, all three papers indicate that both the polarization and AFD rotation angle are reduced by the huge ES around T_N. As explained in Supplemental Material [18], we convert the preliminary neutron-scattering data to the change of the SD polarization at T_N using Ginzburg-Landau free energies. With spin ordering [Fig. 3(d)], Fe and Bi move −0.010 and −0.0095 Å, respectively, and induce polarizations $\Delta P(\text{Fe}) = -1.7 \mu C/cm^2$ and $\Delta P(\text{Bi}) = -1.3 \mu C/cm^2$. The net induced polarization $P_{tot} = \Delta P(\text{Fe}) + \Delta P(\text{Bi}) = -3.0 \mu C/cm^2$ is in excellent agreement with neutron-scattering measurements.

Intriguingly, both Bi and Fe shift with the spin ordering. Fe moves antiparallel to reduce the FE polarizations because AFM ordering favors 180° displacements by the GK rules [24]. The reduction in the Fe polarizations simultaneously reduces the Bi polarization. Consequently, the magnitude of the net polarization is greater than any previously-reported SD polarization (0.29 $\mu C/cm^2$ in $CaMn_7O_{12}$ [26] and 0.36 $\mu C/cm^2$ in $GdMn_2O_5$ [25]).

We have also discovered another huge but hidden ES due to AFD rotations that are strongly coupled to the FE-driven ES. Obviously, this contribution cannot be easily measured, because AFD rotations do not break global inversion symmetry and do not produce a net macroscopic polarization. However, AFD rotations do break local inversion symmetry, and their associated atomic displacements appear in the neutron-scattering data in Fig. 3(e).
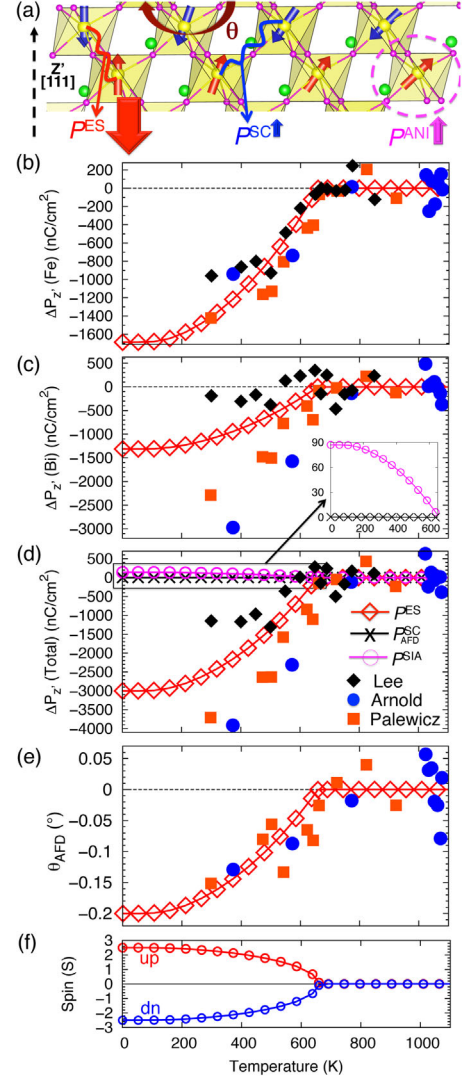
FIG. 3 (color online). (a) SD polarizations along $\mathbf{z}'$ and AFD rotations perpendicular to $\mathbf{z}'$. (b) Calculated Fe polarizations along $\mathbf{z}'$ induced by ES (P^{ES}) compared with measurements by Lee *et al.* [6], Arnold *et al.* [8], and Palewicz *et al.* [12]. (c) Bi polarizations along $\mathbf{z}'$ induced by ES. (d) Total SD polarization $\Delta P_{z'}(\text{Fe}) + \Delta P_{z'}(\text{Bi})$. The inset is the SC polarization calculated from Eqs. (21) and (22) and Ref. [25]. (e) Change of AFD-rotation angle induced by ES. (f) AFM spin ordering versus temperature calculated by mean-field theory.

Based on the good agreement between our predictions and neutron-scattering results, we conclude that the AFD rotation angle is suppressed by ES. Both the polarization and AFD reduction can be understood in terms of the GK rules [24]: AFM ordering decreases bond angles, which reduces the FE polarization and AFD rotations. Because of the recent advancements in local polarization measurements [27], it may soon be possible to directly image the spin-driven structural modification of the AFD.

Although some calculations predict polarizations $\sim 6 \mu C/cm^2$ [28,29] for orthorhombic perovskites such as $HoMnO_3$, the largest measured SD polarization prior to this

work was found in pressurized $TbMnO_3$, where $P = 1.0 \ \mu C/cm^2$ can rise to 1.8 $\mu C/cm^2$ with 5.2 GPa [30] at 5 K. We have checked the possible SD polarization in another type-I multiferroic, $BiCoO_3$, from neutron scattering [31]. But its polarization appears to be smaller than that of $BiFeO_3$ by one order of magnitude. Hence, the type-I multiferroic $BiFeO_3$ unexpectedly exhibits the largest ever SD polarization ($\sim 3 \ \mu C/cm^2$) at room temperature. There are three reasons for this huge SD polarization. First, the exchange interactions and their response to external perturbations such as the electric field or temperature are larger than for the DM interactions, as shown in Tables I and II. Second, even if the ES coefficients were the same for $BiFeO_3$ and the above manganites, the enhanced spin correlation function ($|\langle \mathbf{S}_i \cdot \mathbf{S}_j \rangle| = S^2 = 6.25$) in $BiFeO_3$ and 2.25 in the manganites) would strongly enhance the ESP in $BiFeO_3$. Third, in contrast to the E-type ordering in the manganites, the almost antiparallel alignment of neighboring spins in $BiFeO_3$ also enhances the ESP.

The greatest advantages of $BiFeO_3$ are its large FE polarization, high T_c, and high T_N above room temperature. These advantages have unfortunately hampered precise characterizations of the ME polarizations around T_N. Leakage currents at high temperatures and the preexisting large FE polarization have hidden the SD ME polarizations at T_N. Fortunately, intrinsic measurements such as neutron scattering, Raman spectroscopy, and directional dichroism have recently begun uncovering the hidden ME couplings of $BiFeO_3$. So, in addition to having the largest known FE polarization, $BiFeO_3$ may also have SD polarizations much larger than any other known material. Our systematic approach will greatly aid further exploration of hidden but possibly large spin-driven polarizations and their ME origins in other type-I multiferroics.

[*] jjjun97@gmail.com

[1] J. R. Teague, R. Gerson, and W. J. James, Solid State Commun. **8**, 1073 (1970).

[2] I. Sosnowska, T. Peterlin-Neumaier, and E. Steichele, J. Phys. C **15**, 4835 (1982).

[3] M. Tokunaga, M. Azuma, and Y. Shimakawa, J. Phys. Soc. Jpn. **79**, 064713 (2010).

[4] J. Park et al., J. Phys. Soc. Jpn. **80**, 114714 (2011).

[5] A. M. Kadomtseva, A. K. Zvezdin, Yu. F. Popv, A. P. Pyatakov, and G. P. Vorob'ev, JETP Lett. **79**, 571 (2004); D. Lebeugle, D. Colson, A. Forget, M. Viret, A. M. Bataille, and A. Goukasov, Phys. Rev. Lett. **100**, 227602 (2008); M. Ramazanoglu, W. Ratcliff II, Y. J. Choi, S. Lee, S.-W. Cheong, and V. Kiryukhin, Phys. Rev. B **83**, 174434 (2011).

[6] S. Lee et al., Phys. Rev. B **88**, 060103(R) (2013).

[7] T. Kimura, T. Goto, H. Shintani, K. Ishizaka, T. Arima, and Y. Tokura, Nature (London) **426**, 55 (2003).

[8] D. C. Arnold, K. S. Knight, F. D. Morrison, and P. Lightfoot, Phys. Rev. Lett. **102**, 027602 (2009).

[9] J. Jeong et al., Phys. Rev. Lett. **108**, 077202 (2012); M. Matsuda, R. S. Fishman, T. Hong, C. H. Lee, T. Ushiyama, Y. Yanagisawa, Y. Tomioka, and T. Ito, Phys. Rev. Lett. **109**, 067205 (2012); Z. Xu et al., Phys. Rev. B **86**, 174419 (2012).

[10] M. Cazayous, Y. Gallais, A. Sacuto, R. deSousa, D. Lebeugle, and D. Colson, Phys. Rev. Lett. **101**, 037601 (2008); P. Rovillain R. de Sousa, Y. Gallais, A. Sacuto, M. A. Méasson, D. Colson, A. Forget, M. Bibes, A. Barthélémy, and M. Cazayous, Nat. Mater. **9**, 975 (2010).

[11] D. Talbayev, S. A. Trugman, S. Lee, H. T. Yi, S.-W. Cheong, and A. J. Taylor, Phys. Rev. B **83**, 094403 (2011); U. Nagel, R. S. Fishman, T. Katuwal, H. Engelkamp, D. Talbayev, H. T. Yi, S.-W. Cheong, and T. Rõõm, Phys. Rev. Lett. **110**, 257201 (2013).

[12] A. Palewicz, R. Przenioslo, I. Sosnowska, and A. W. Hewat, Acta Crystallogr. Sect. B **63**, 537 (2007).

[13] G. A. Smolenskii and I. E. Chupis, Usp. Fiz. Nauk **137**, 415 (1982).

[14] A. P. Pyatakov and A. K. Zvezdin, Eur. Phys. J. B **71**, 419 (2009).

[15] R. S. Fishman, Phys. Rev. B **87**, 224419 (2013).

[16] R. S. Fishman, J. T. Haraldsen, N. Furukawa, and S. Miyahara, Phys. Rev. B **87**, 134416 (2013).

[17] J. Íñiguez, Phys. Rev. Lett. **101**, 117201 (2008).

[18] See Supplemental Material at http://link.aps.org/supplemental/10.1103/PhysRevLett.115.207203 for theoretical details, which includes Refs. [18–23].

[19] R. D. King-Smith and D. Vanderbilt, Phys. Rev. B **47**, 1651 (1993).

[20] K. Momma and F. Izumi, J. Appl. Crystallogr. **44**, 1272 (2011).

[21] C. Weingart, N. Spaldin, and E. Bousquet, Phys. Rev. B **86**, 094413 (2012).

[22] P. E. Blöchl, Phys. Rev. B **50**, 17953 (1994); G. Kresse and D. Joubert, Phys. Rev. B **59**, 1758 (1999).

[23] J. T. Zhang, X. M. Lu, J. Zhou, H. Sun, F. Z. Huang, and J. S. Zhu, Phys. Rev. B **87**, 075127 (2013).

[24] J. B. Goodenough, Magnetism and the Chemical Bond (Wiley, New York, 1993).

[25] N. Lee, C. Vecchini, Y. J. Choi, L. C. Chapon, A. Bombardi, P. G. Radaelli, and S-W. Cheong, Phys. Rev. Lett. **110**, 137203 (2013).

[26] R. D. Johnson, L. C. Chapon, D. D. Khalyavin, P. Manuel, P. G. Radaelli, and C. Martin, Phys. Rev. Lett. **108**, 067201 (2012).

[27] C. L. Jia, S.-B. Mi, K. Urban, I. Vrejoiu, M. Alexe, and D. Hesse, Nat. Mater. **7**, 57 (2008); M. F. Chisholm, W. D. Luo, M. P. Oxley, S. T. Pantelides, and H. N. Lee, Phys. Rev. Lett. **105**, 197602 (2010).

[28] I. A. Sergienko, C. Sen, and E. Dagotto, Phys. Rev. Lett. **97**, 227204 (2006).

[29] S. Picozzi, K. Yamauchi, B. Sanyal, I. A. Sergienko, and E. Dagotto, Phys. Rev. Lett. **99**, 227201 (2007).

[30] T. Aoyama, K. Yamauchi, A. Iyama, S. Picozzi, K. Shimizu, and T. Kimura, Nat. Commun. **5**, 4927 (2014).

[31] A. A. Belik et al., Chem. Mater. **18**, 798 (2006).